Human Molecular Genetics, 2011, Vol. 20, No. 5 **948–961**
doi:10.1093/hmg/ddq541
Advance Access published on December 13, 2010

A Phe377del mutation in ANK leads to impaired osteoblastogenesis and osteoclastogenesis in a mouse model for craniometaphyseal dysplasia (CMD)

I-Ping Chen[1], Liping Wang[2], Xi Jiang[2], Hector Leonardo Aguila[3] and Ernst J. Reichenberger[2,*]

[1]Department of Oral Health and Diagnostic Sciences, School of Dental Medicine, [2]Department of Reconstructive Sciences, School of Dental Medicine and [3]Department of Immunology, University of Connecticut Health Center, Farmington, CT 06030, USA

Received April 7, 2010; Revised and Accepted December 8, 2010

Craniometaphyseal dysplasia (CMD) is a rare genetic disorder with hyperostosis of craniofacial bones and widened metaphyses in long bones. Patients often suffer from neurological symptoms due to obstruction of cranial foramina. No proven treatment is available and the pathophysiology is largely unknown. A Phe377 ($TTC_{1130-1132}$) deletion in exon 9 of the pyrophosphate (PPi) transporter ANK leads to CMD-like features in an $Ank^{KI/KI}$ mouse model. Here, we investigated the effects of CMD-mutant ANK on mineralization and bone mass at a cellular level. $Ank^{KI/KI}$ osteoblast cultures showed decreased mineral deposition. Expression of bone mineralization regulating genes *Mmp13*, *Ocn*, *Osx* and *Phex* was reduced in $Ank^{KI/KI}$ osteoblasts, while the *Fgf23* mRNA level was highly elevated in $Ank^{KI/KI}$ calvarial and femoral bones. Since ANK is a known PPi transporter, we examined other regulators of Pi/PPi homeostasis *Enpp1* and *Tnap.* Significantly increased ENPP1 activity may compensate for dysfunctional mutant ANK leading to comparable extracellular PPi levels in $Ank^{+/+}$ osteoblasts. Similar to $Ank^{KI/KI}$ bone marrow-derived macrophage cultures, peripheral blood cultures from CMD patients exhibited reduced osteoclastogenesis. Cell-autonomous effects in $Ank^{KI/KI}$ osteoclasts resulted in disrupted actin ring formation and cell fusion. In addition, $Ank^{KI/KI}$ osteoblasts failed to adequately support osteoclastogenesis. Increased bone mass could partially be rescued by bone marrow transplants supporting our hypothesis that reduced osteoclastogenesis contributes at least in part to hyperostosis. We conclude that the Phe377del mutation in ANK causes impaired osteoblastogenesis and osteoclastogenesis resulting in hypomineralization and a high bone mass phenotype.

INTRODUCTION

The term craniometaphyseal dysplasia (CMD) was coined by Jackson *et al.* (1) in 1954 for a rare disorder involving progressive thickening of skulls and widening of metaphyses of tubular bones throughout the life. Other reported abnormalities of CMD include maxillary retrusion, mandibular prognathism and hyperostosis of jawbones (2–4). CMD can be diagnosed early in infancy due to difficulties with feeding and breathing caused by obstruction of the nasal lumen (5–7). Hyperostosis of the skull leads to narrowing of cranial foramina and obstruction of cranial nerves II, III, VI, VII and VIII by bony encroachment (8–10). Symptomatic Chiari I malformation, characterized by displacement of the cerebellar tonsils beneath the foramen magnum into the cervical spinal cord, has been reported (11,12). Treatment of CMD is limited to surgical intervention for decompression of obstructed foramina, to slow progression of facial paralysis, to reduce visual and auditory disturbances and to improve facial appearance.

The little we know about the pathophysiology of CMD is mainly based on a few case reports. Histopathological

*To whom correspondence should be addressed at: Department of Regenrative Medicine, Center for Restorative Medicine and Skeletal Development, University of Connecticut Health Center (UCHC), 263 Farmington Avenue, Farmington, CT 06030-3705, USA. Tel: +1 8606792062; Fax: +1 8606792910; Email: reichenberger@uchc.edu

studies of CMD patients showed inconsistent findings, which include increased numbers of osteoblasts (1,13), no osteoclasts in the endosteal or periosteal layers (14), hyperostotic bone with defective mineralization of bone matrix (15), elevated numbers of osteoclasts and osteoclastic surface area (16) and increased bone formation and bone resorption (17). Yamamoto *et al.* (18) reported lack of expression of a vacuolar proton pump in osteoclasts of a single CMD patient. From these reports, it is unclear how osteoblastogenesis and osteoclastogenesis in CMD patients are affected.

CMD occurs sporadically or is transmitted as an autosomal dominant (AD) or autosomal recessive (AR) trait. Mutations located in cytoplasmic domains close to the C-terminus of the human *ANK* gene (*ANKH*) were identified for the AD form of CMD (19,20). Database searches with the full-length mouse *Ank* gene have shown a high degree of sequence conservation among vertebrates, including zebrafish, rats, mice and human, indicating that ANK may play a crucial role in physiological processes (20,21). Although the topology of the ANK protein has not been experimentally confirmed and the precise structure of ANK is still unknown, ANK is proposed to act as a pyrophosphate (PPi) transporter to channel intracellular PPi into extracellular matrix (21). Extracellular PPi (ePPi) in a physiological concentration acts as a potent inhibitor of mineralization. Low concentrations of ePPi lead to excess hydroxyapatite (HA) deposition, while supersaturation of ePPi promotes calcium pyrophosphate dihydrate (CPPD) crystal formation. On the other hand, Pi is a major component and a promoter of HA formation. A tightly controlled balance between ePi and ePPi is required to maintain normal bone mineral content.

Homeostasis of Pi/PPi is primarily maintained by the concerted activities of ANK and other regulators: PC-1 (plasma cell membrane glycoprotein 1, protein encoded by *Enpp1*), which generates PPi from extracellular and intracellular nucleoside triphosphate (ATP) and TNAP (protein encoded by *Tnap*), which hydrolyzes ePPi to generate Pi. Deficiency of any of these three proteins can lead to mineral-related pathological conditions in bone. Tiptoe walking (*ttw/ttw*) mice carry a naturally occurring nonsense mutation in PC-1 and develop accelerated bone formation as well as ectopic ossification in spinal and periarticular ligaments (22). *Tnap* knock-out mice ($Akp2^{-/-}$), on the other hand, replicate features of human infantile hypophosphatasia, including rachitic changes, osteopenia and spontaneous fracture (23). $Ank^{ank/ank}$ and $Ank^{null/null}$ mice, which are lacking functional ANK protein, show progressive arthritic destruction of joints with increased HA deposition eventually leading to complete rigidity and death around 6 months of age (24–26). Interestingly, $Ank^{null/null}$ mice exhibit some characteristic features seen in CMD patients such as increased thickness of skull bones, fusion of middle-ear bones, narrowing of foramen magnum and decreased trabeculation of metaphyses in femurs (27). However, $Ank^{null/null}$ mice do not replicate obliteration of nasal sinuses, mandibular prognathism with massive jawbones, hypertelorism and flaring metaphyses in long bones. Differences in phenotype between human CMD and $Ank^{null/null}$ mice suggest that the mechanism of *ANKH* mutations leading to CMD in humans is not merely a loss of function of PPi transport.

We have generated a knock-in (KI) mouse model for CMD expressing a human ANK mutation (Phe377 deletion), which develop many of the features that are characteristic for CMD patients (28). These mice exhibit increased bone mass in craniofacial bones, especially the mandibles and excessive trabecular bone in diaphyses of long bones, while metaphyses are undertrabeculated. Surprisingly, the cortex of $Ank^{KI/KI}$ long bones is hypomineralized. Although histomorphometry indicated increased osteoclast number in $Ank^{KI/KI}$ mice, the *in vitro* cultures showed decreased osteoclastogenesis (28). Here, we investigate the effects of the Phe377del mutation of ANK on osteoblastogenesis and osteoclastogenesis at a cellular level in the *Ank* KI mouse model.

RESULTS

Effects of Phe377del Ank mutation on osteoblastogenesis

To study the mutational effects on bone, we first compared wild-type and mutant *Ank* RNA levels in calvarial and femoral bones and examined whether *Ank* expression was modulated *in vitro* during calvarial osteoblast differentiation by quantitative PCR (Fig. 1A and B). While there was no statistical difference in spatial *Ank* expression of calvarial and femoral bones from $Ank^{+/+}$ and $Ank^{KI/KI}$ mice, we detected an increase in temporal *Ank* expression at later stages of differentiating $Ank^{+/+}$ and $Ank^{KI/KI}$ osteoblast cultures. The *Ank* expression in calvarial osteoblasts showed a statistically significant increase after culturing in osteogenic media for 7, 14 and 21 days. The level of *Ank* mRNA increase *in* $Ank^{+/+}$ and $Ank^{KI/KI}$ osteoblast cultures was comparable.

Dysregulation of osteoblastogenesis can result from abnormal proliferation, apoptosis or osteoblast differentiation. We have observed no significant difference in cell proliferation and apoptosis in $Ank^{+/+}$ and $Ank^{KI/KI}$ mice *in vivo* or in calvarial osteoblast cultures by BrdU and TUNEL assays (data not shown) but found decreased mineral density in the cortical bone of $Ank^{KI/KI}$ femurs. We therefore examined matrix and mineral deposition *in vitro*. $Ank^{KI/KI}$ calvarial osteoblast cultures [mouse calvarial osteoblast (mCOB)] in osteogenic medium produced less mineral nodules over a 21-day culture period, but alkaline phosphatase (ALP) staining showed no apparent difference (Fig. 1C). Subsequent staining with crystal violet indicated that the cell density in all plates reached confluence and there was no difference in DNA content between $Ank^{+/+}$ and $Ank^{KI/KI}$ cultures by the PicoGreen assay (Supplementary Material, Table S1).

$Ank^{KI/KI}$ bone marrow stromal cell cultures (BMSCs) also contained significantly fewer ALP-positive cell clusters than $Ank^{+/+}$ cultures, which was likely due to a decreased number of adherent cell colonies as shown by crystal violet staining (Fig. 1D and E). We next visualized the mineral nodule deposition by alizarin red S staining and quantified calcium binding to alizarin red by colorimetric detection as an indicator for calcification (Fig. 1F). A significant decrease in the mineral nodule formation was found in $Ank^{KI/KI}$ BMSCs. Mineralization in $Ank^{KI/KI}$ BMSC cultures was ~14-fold decreased, while crystal violet staining and ALP staining were only 3-fold decreased, which indicates that the BMSCs that are present have a poor mineralization capacity,

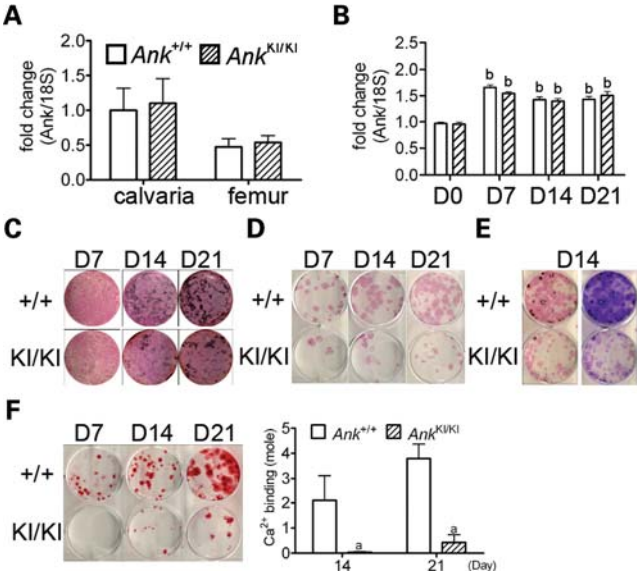

Figure 1. *Ank* expression, matrix and mineral formation in osteoblast cultures. qPCR of *Ank* expression (**A**) in calvarial and femoral bone and (**B**) during *in vitro* calvarial osteoblast differentiation. Data were normalized to 18S RNA. Data presented are average with SD from three independent experiments. $^{b}P < 0.01$ indicates significant difference in fold-change compared with $Ank^{+/+}$ calvarial osteoblasts at day 0. Expression in $Ank^{+/+}$ calvaria and $Ank^{+/+}$ calvarial osteoblasts at day 0 were used as calibrators. No difference between $Ank^{+/+}$ and $Ank^{KI/KI}$ groups at any time point. (**C**) $Ank^{+/+}$ and $Ank^{KI/KI}$ mCOBs stained for ALP and von Kossa at culture days 7, 14 and 21. $Ank^{KI/KI}$ cultures show reduced mineral nodule formation. (**D**) $Ank^{+/+}$ and $Ank^{KI/KI}$ BMSCs stained for ALP at culture days 7, 14 and 21. (**E**) $Ank^{+/+}$ and $Ank^{KI/KI}$ BMSCs stained for ALP followed by von Kossa staining (left panel) and crystal violet (right panel) at day 14. (**F**) $Ank^{+/+}$ and $Ank^{KI/KI}$ BMSCs stained for alizarin red S at culture days 7, 14 and 21. Histogram represents corresponding calcium-binding levels. $^{a}P < 0.05$ indicates significant difference.

which is consistent with results from calvarial osteoblast cultures.

Regulation of ePPi level in $Ank^{KI/KI}$ osteoblasts

ANK has been proposed to act as a PPi transporter to channel intracellular PPi to the extracellular matrix (21). ePPi is an inhibitor for HA deposition during physiological bone mineralization. Since we observed a hypomineralized phenotype in $Ank^{KI/KI}$ mice and in osteoblast cultures, abnormal ePPi levels were a possible reason for abnormal HA crystal deposition. We compared the ePPi levels of cultured $Ank^{+/+}$ and $Ank^{KI/KI}$ calvarial osteoblasts and surprisingly, we found no significant difference between the two groups (Fig. 2A, left panel). In $Ank^{null/null}$ cells, which lack ANK protein, the ePPi level was, as expected, significantly lower than in wild-type cultures (Fig. 2A, right panel). The difference in the absolute ePPi levels in wild-type controls of the $Ank^{KI/KI}$ and $Ank^{null/null}$ groups may be due to differences in their genetic background. We next examined whether other PPi regulators participate in balancing the ePPi level in $Ank^{KI/KI}$ calvarial osteoblasts.

Tightly balanced extracellular Pi and PPi levels are coregulated by PC-1, ANK and TNAP in osteoblasts. Whether these three proteins work independently in $Ank^{KI/KI}$ mice or in concert is unknown. To determine whether *Tnap*/TNAP or *Enpp1*/PC-1 are affected by the Phe377del mutation in ANK, we first examined the expression of *Tnap* and *Enpp1* mRNA messages and found increased *Tnap* and *Enpp1* expression in differentiating osteoblasts; however, we detected no significant difference in expression levels between $Ank^{+/+}$ and $Ank^{KI/KI}$ cultures (Fig. 2B). We then measured the enzymatic activity of TNAP and PC-1 in mCOBs at different stages of osteoblast differentiation. Cell lysates from $Ank^{+/+}$ and $Ank^{KI/KI}$ mCOBs were colorimetrically assessed for TNAP and PC-1 activity. PC-1 activity was significantly higher in $Ank^{KI/KI}$ cultures at days 14 and 21, while TNAP activity was comparable between $Ank^{+/+}$ and $Ank^{KI/KI}$ cultures (Fig. 2C). ePPi levels measured on day 14 and day 21 $Ank^{+/+}$ and $Ank^{KI/KI}$ cultures showed no significant differences (Supplementary Material, Fig. S1). Because the increased PC-1 activity did not result in increased ePPi levels in $Ank^{KI/KI}$ osteoblasts, these results suggest that PC-1 may be post-transcriptionally regulated and may compensate for reduced PPi transport by mutant ANK.

Decreased $Ank^{KI/KI}$ osteoblast marker gene expression at late differentiation stages

To examine whether the Phe377del mutation in ANK affects expression of osteoblast differentiation markers, we performed quantitative real-time PCR (qPCR) of samples isolated from 0-, 7-, 14- and 21-day $Ank^{+/+}$ and $Ank^{KI/KI}$ mCOB cultures grown in the osteogenic medium. We found that mRNA isolated from day 21 $Ank^{KI/KI}$ cultures showed reduced expression of *Mmp13*, *Ocn*, *Runx2* and *Sp7*, while other osteoblast marker genes including *ColI*, *Bsp* and *Opn* showed comparable levels in $Ank^{+/+}$ and $Ank^{KI/KI}$ cells (Fig. 3A, Supplementary Material, Table S2). We detected no significant differences in gene expression between $Ank^{+/+}$ and $Ank^{KI/KI}$ early-stage osteoblasts (Supplementary Material, Table S2). We also examined the expression of these marker genes in RNA isolated from 8- to 10-week-old calvarial and femoral bones and found no significant differences between $Ank^{+/+}$ and $Ank^{KI/KI}$ mice (Supplementary Material, Table S2). A possible explanation may be that the differentiation stages of osteoblasts are heterogeneous in bone, while the populations are somewhat more homogeneous in culture systems at days 0, 7, 14 and 21. Interestingly, *Phex* (phosphate regulating gene with homologies to endopeptidases on the X chromosome) was also significantly decreased in $Ank^{KI/KI}$ osteoblast cultures (Fig. 3A). An inactivating mutation of *Phex* is known to cause X-linked hypophosphatemia (XLH) in humans and impaired mineralization of bone and dentin in *Hyp* mice (29–32). Changes in expression levels of late-stage marker genes suggest that mutant *Ank* negatively affects osteoblasts at late stages of differentiation and partially explains the poor mineralization potential of $Ank^{KI/KI}$ osteoblast cultures.

Several bone-derived factors like *Dmp1*, *Mepe*, *Phex* and *Fgf23* coordinately regulate bone mineralization. These messages are expressed in late-stage osteoblasts and mainly in osteocytes. We examined gene expression of isolated RNA from 8- to 10-week-old calvarial and femoral bones by qPCR and observed significant increases of *Fgf23* expression in both, $Ank^{KI/KI}$ calvarial and femoral bone (Fig. 3B and C). Increased *Dmp1* was found only in $Ank^{KI/KI}$ calvariae,

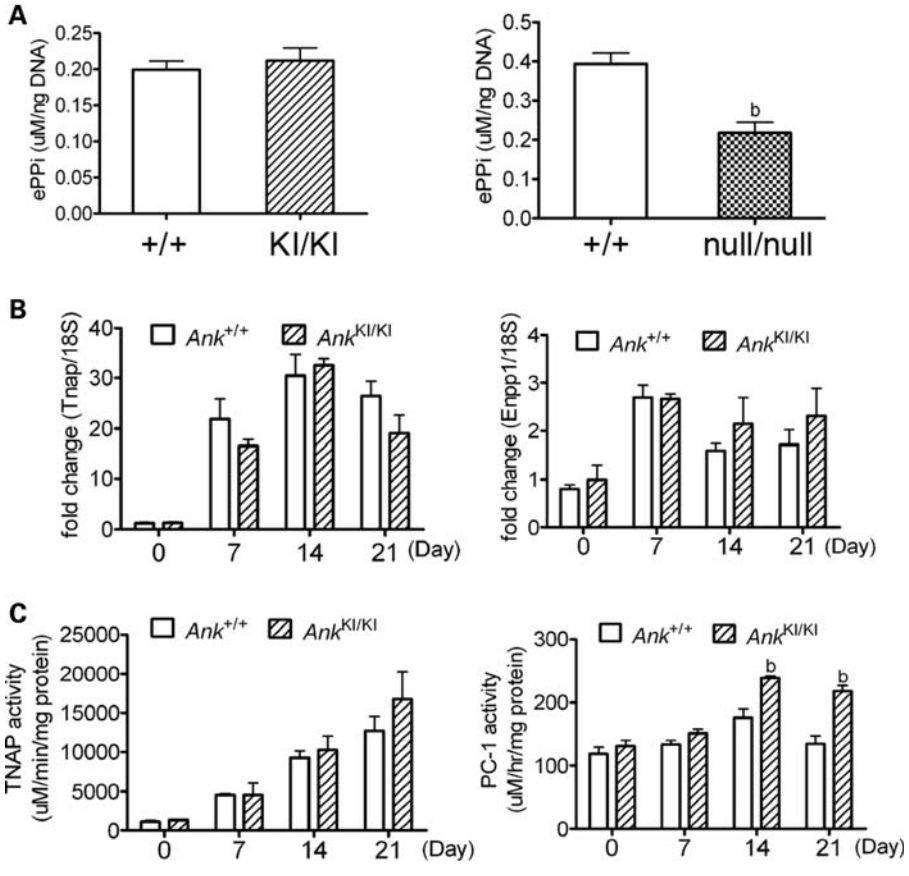

Figure 2. Effects of Phe377del *Ank* on ePPi and on regulators for ePPi, *Tnap* and *Enpp1* in mCOBs. (**A**) ePPi assays in $Ank^{+/+}$ and $Ank^{KI/KI}$ mCOBs (left panel) as well as in wild-type and $Ank^{null/null}$ mCOBs (right panel). Statistical analysis was performed by Student's *t*-test. $^{b}P < 0.01$. (**B**) Gene expression analysis by qPCR of *Tnap* and *Enpp1* in $Ank^{+/+}$ and $Ank^{KI/KI}$ mCOBs in differentiation medium for 0, 7, 14 and 21 days. No significant difference was found between $Ank^{+/+}$ and $Ank^{KI/KI}$ cultures during osteoblast differentiation. (**C**) Enzymatic activities of TNAP and PC-1 in cultured $Ank^{+/+}$ and $Ank^{KI/KI}$ mCOBs at days 0, 7, 14 and 21. $^{b}P < 0.01$ indicates statistical significance by one-way ANOVA.

possibly due to the hyperostotic phenotype and *Phex* expression was not significantly changed in calvariae and femurs. Interestingly, *Mepe* was increased in $Ank^{KI/KI}$ calvariae (Fig. 3B) but decreased in femurs (Fig. 3C). It is unclear whether the differential expression of *Mepe* between calvarial and femoral bones reflect the differences between intramembranous and endochondral bone formation in $Ank^{KI/KI}$ mice.

FGF23 can regulate bone mineralization via a systemic effect through interaction with KLOTHO in the kidney (33,34) or via local effects in the bone environment where *Fgf23* is expressed (35). Overexpression of FGF23 suppresses not only osteoblast differentiation but also matrix mineralization in fetal rat calvarial cell cultures (36). Furthermore, overexpression of *Fgf23* in transgenic mice results in hypomineralization of bone and in hypophosphatemia (33). Because of the remarkably increased *Fgf23* levels, we next examined whether serum levels of calcium and phosphate are affected in $Ank^{KI/KI}$ mice.

Lower calcium and phosphorus serum levels in $Ank^{KI/KI}$ mice

We first measured serum calcium, phosphorus and PTH levels in $Ank^{+/+}$ and $Ank^{KI/KI}$ mice at the age of 6 weeks. $Ank^{KI/KI}$ mice showed lower calcium ($Ank^{+/+} = 9.334 \pm 0.717$ mg/dl, $n = 9$; $Ank^{KI/KI} = 8.962 \pm 0.415$ mg/dl, $n = 9$; $P < 0.05$) and phosphorus levels ($Ank^{+/+} = 6.622 \pm 1.102$ mg/dl, $n = 10$; $Ank^{KI/KI} = 5.494 \pm 0.893$ mg/dl, $n = 11$; $P < 0.05$) when compared with their wild-type littermates. At the same age, serum PTH levels were inappropriately normal or increased in $Ank^{KI/KI}$ mice ($Ank^{+/+} = 165.02 \pm 81.063$ pg/ml, $n = 9$; $Ank^{KI/KI} = 171.413 \pm 156.842$ pg/ml, $n = 8$; $P = 0.915$). Interestingly, the serum phosphorus level was normalized in 10-week-old male $Ank^{KI/KI}$ mice ($Ank^{+/+} = 3.716 \pm 0.667$ mg/dl, $n = 7$; $Ank^{KI/KI} = 4.248 \pm 0.651$ mg/dl, $n = 8$;$P = 0.142$) while the calcium level remained significantly lower ($Ank^{+/+} = 9.591 \pm 0.833$ mg/dl, $n = 7$; $Ank^{KI/KI} = 8.829 \pm 0.324$ mg/dl, $n = 8$; $P < 0.05$). These data indicate that mutant *Ank* participates in the regulation of metabolic activities in $Ank^{KI/KI}$ mice and that decreased phosphorus levels were potentially corrected by a feedback mechanism as the mice aged.

Local factors in bone are major contributors to skeletal abnormalities in $Ank^{KI/KI}$ mice

Characteristic features of bones are determined by local factors synthesized within a bone and by systemic factors,

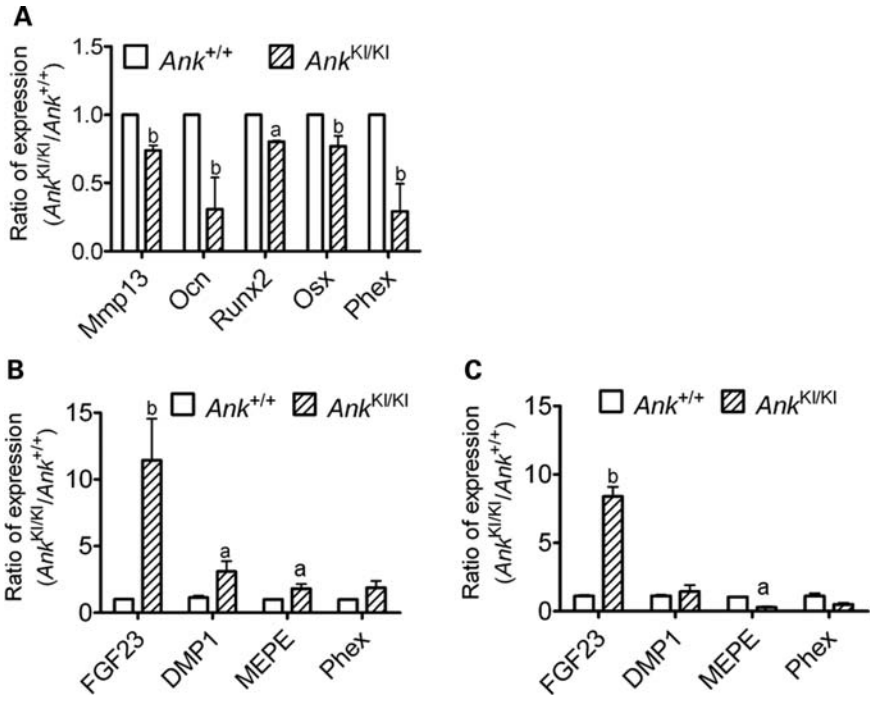

Figure 3. Gene expression in mCOBs and bone tissues from $Ank^{+/+}$ and $Ank^{KI/KI}$ mice. (**A**) qPCR of decreased *Mmp13*, *Ocn*, *Runx2*, *Sp7 (Osx)* and *Phex* in day 21 $Ank^{KI/KI}$ calvarial osteoblast cultures normalized to expression levels of $Ank^{+/+}$ cells. Data from three independent experiments were pooled. $^{a}P < 0.05$, $^{b}P < 0.01$. (**B**) qPCR analysis of *Fgf23*, *DMP1*, *MEPE* and *Phex* in calvariae and (**C**) in femurs. RNA samples isolated from 8- to10-week-old $Ank^{+/+}$ and $Ank^{KI/KI}$ mice.

such as externally produced hormones, cytokines or other factors. Since we found defects intrinsic to $Ank^{KI/KI}$ osteoblasts and osteoclasts as well as abnormal serum phosphorus and calcium, we wanted to determine whether local factors in bone or systemic factors are major contributors to the CMD-like skeletal phenotype in $Ank^{KI/KI}$ mice using reciprocal bone explantation (37,38).

Radiographic images of 4.5-day-old femurs of $Ank^{+/+}$ and $Ank^{KI/KI}$ donor mice showed that they were very similar in shape and trabeculation (Fig. 4). One $Ank^{+/+}$ and one $Ank^{KI/KI}$ femur were transplanted into the lateral back muscles (one femur each side) of 4-week-old $Ank^{+/+}$ and $Ank^{KI/KI}$ recipient mice. Transplanted bones were harvested and analyzed when the mice were 7 weeks old because we had previously observed lower serum calcium and phosphorus levels in $Ank^{KI/KI}$ mice at the age of 6 weeks. Wild-type bones transplanted into wild-type mice and $Ank^{KI/KI}$ bones into $Ank^{KI/KI}$ mice maintained their phenotypic characteristics and grew in size, which suggests that surgical procedures were not a factor interfering with data interpretation. Since we had previously found extensive trabeculation in diaphyses of $Ank^{KI/KI}$ mice (28), we measured the bone volume of diaphyses by μCT. We chose measuring diaphyseal bone volume rather than metaphyseal bone volume because growth plates are easily damaged during resection from back muscles and may skew measurements. Our results showed that $Ank^{KI/KI}$ femurs transplanted into $Ank^{KI/KI}$ mice developed significantly more bone volume than $Ank^{+/+}$ bones explanted into either $Ank^{+/+}$ or $Ank^{KI/KI}$ mice (Fig. 4). We also found increased diaphyseal bone in $Ank^{KI/KI}$ bones transplanted into $Ank^{+/+}$ mice compared with $Ank^{+/+}$ bones that were transplanted into $Ank^{+/+}$ or $Ank^{KI/KI}$ recipient mice; however, the difference was not statistically significant (Fig. 4). Because $Ank^{KI/KI}$ bones that were transplanted into $Ank^{+/+}$ mice had less trabecular bone deposition in diaphyses than transplanted into $Ank^{KI/KI}$ mice, it appears that the influence of hormonal (systemic) factors cannot be ruled out. However, based on the observation that $Ank^{KI/KI}$ bones developed the abnormal bone shape as well as excessive diaphyseal trabeculation when transplanted into both, wild-type and mutant recipient animals, we suggest that local factors play a more important role in the development of a CMD-like skeletal phenotype.

Decreased osteoclastogenesis in peripheral blood cultures of CMD patients

We have shown that mouse $Ank^{KI/KI}$ bone marrow-derived macrophage (BMM) cultures form significantly fewer and smaller osteoclasts during *in vitro* osteoclast differentiation and have significantly reduced mineral resorption on calcium-phosphate-coated slides as well as on bone chips (28). To examine whether similar findings can be observed in CMD patients, we compared osteoclasts derived from peripheral blood mononuclear cells of adult CMD patients to age- and sex-matched healthy controls. Cultures from CMD patients formed less $TRAP^{+}$ multinucleated cells and resorbed less mineral on osteologic slides (Fig. 5A and B). Although the number of samples (patients $n = 2$; controls $n = 7$) is small due to the rarity of the disorder, the outcome is perfectly in line with previous findings in $Ank^{KI/KI}$ mice suggesting that osteoclastogenesis in CMD patients is impaired by mutant ANK.

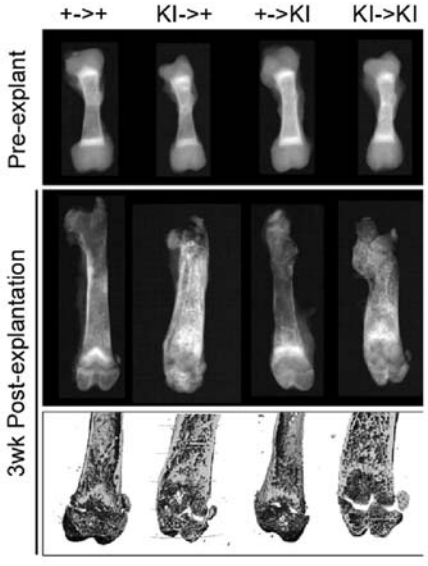

	+ -> +	KI -> +	+ -> KI	KI -> KI
Bone vol. (mm^3)	0.83±0.14	1.42±0.59	0.86±0.47	1.69±0.28[ab]

Figure 4. Bone explantation in $Ank^{+/+}$ (+/+) and $Ank^{KI/KI}$ (KI/KI) mice. (**A**) X-ray and μCT images of femurs prior to and 3 weeks after intramuscular explantation. $Ank^{+/+}$ (+) and $Ank^{KI/KI}$ (KI) femurs explanted into (→) $Ank^{+/+}$ and $Ank^{KI/KI}$ mice. The Table shows trabecular bone volume in femoral diaphyses ($n = 6$ per group). Bone volume of KI/KI bones transplanted into KI/KI recipient mice is significantly larger than bone volume of +/+ bones transplanted into +/+ mice, $^{a}P < 0.05$, and +/+ bones transplanted into KI/KI recipient mice, $^{b}P < 0.05$. Statistics performed by ANOVA.

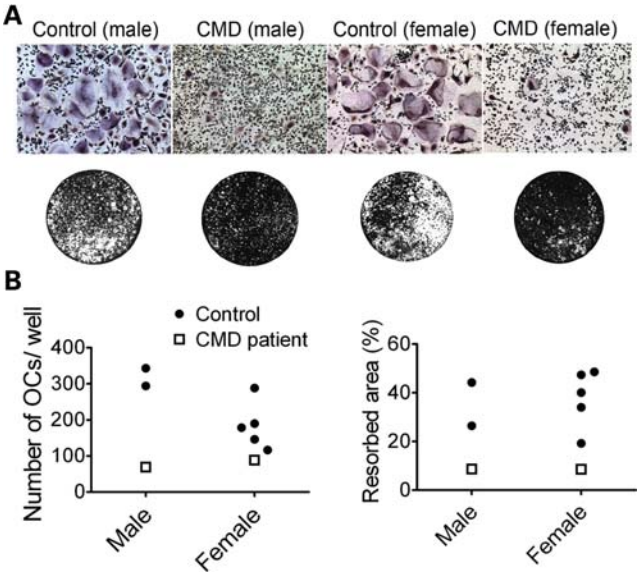

Figure 5. *In vitro* osteoclast assays in human peripheral blood cultures derived from CMD patients and sex- and age-matched healthy controls. (**A**) Representative images of TRAP staining (at day 15) of cultures from CMD patients and controls (top). Resorption assays on calcium-phosphate-coated slides after fixation and von Kossa staining (below). White areas represent the resorbed area, while black areas show the remaining mineralized surface. (**B**) Histograms show number of mature osteoclasts per well and percentile of the resorbed area.

Cell-autonomous effects of Phe377del ANK on $Ank^{KI/KI}$ osteoclasts

To determine whether there is a difference in temporal expression of *Ank* in differentiating osteoclasts, we tested *Ank* expression in RAW264.7 cells, in murine BMM cultures and in an enriched osteoclast progenitor cell population ($CD11b^{-/low}CD45R^{-}CD3^{-}CD115^{high}$) by fluorescent-activated cell sorting (FACS) (39). In all the culture systems, we detected remarkably increased *Ank* levels in mature osteoclasts compared with osteoclast progenitors (Fig. 6A, Supplementary Material, Fig. S1). We conclude that *Ank* may play an important role during osteoclastogenesis, which is confirmed by the *in vitro* observation that the Phe377del ANK mutation leads to impaired osteoclastogenesis in $Ank^{KI/KI}$ mice and in CMD patients.

To determine whether impaired osteoclastogenesis in $Ank^{KI/KI}$ BMMs is caused by cell-autonomous defects in osteoclasts or by reduced numbers of precursors, we examined the percentage of $CD11b^{-/low}CD45R^{-}CD3^{-}CD115^{high}CD117^{high}$ osteoclast precursor populations in bone marrow of $Ank^{+/+}$ and $Ank^{KI/KI}$ mice and observed no significant difference in number (Supplementary Material, Fig. S2). However, mature osteoclasts derived from isolated progenitors of $Ank^{KI/KI}$ BMM cultures presented with reduced cell size, disrupted actin rings (Fig. 6B) and decreased cell migration. The actin ring plays a critical role in bone resorption by forming a seal between the osteoclast and the bone surface (40). Using a live-cell time-lapse imaging system and by quantifying the migratory velocity with MetaMorph software, we observed that movement was greatly reduced in $Ank^{KI/KI}$ BMMs ($Ank^{+/+}$: $Ank^{KI/KI} = 2.25 \pm 0.447$:1 $\pm$ 0.248; $n = 15$; $P < 0.05$). In addition, fusion efficiency in $Ank^{KI/KI}$ BMM cultures (nuclei number of mature osteoclasts divided by total number of nuclei) was decreased (Fig. 6C). The latter observation suggests that less mononuclear cells participate in fusion and maturation of $Ank^{KI/KI}$ osteoclasts in culture. We examined expression levels of osteoclast markers in RNA samples isolated from day 0, 2 and 5 BMM cultures with M-CSF and RANKL stimulation (30 ng/ml). Day 0 mRNA was prepared from untreated freshly isolated BMMs, which contains osteoclast precursors. Samples from day 2 and 5 cultures represent pre-fusion osteoclasts and mature osteoclasts. We did not detect differential expression of *Ank*, *Oscar*, *TRAP, cathepsin K*, *Nfatc1*, *Mmp9, ATP6v0d2* and *AQP9* (data not shown). However, *DC-Stamp*, critical for fusion, was significantly decreased on day 2 of $Ank^{KI/KI}$ BMM cultures (Fig. 6D).

Stimulation by osteoblasts plays a crucial role during osteoclast formation (41,42). To study whether decreased osteoclastogenesis in $Ank^{KI/KI}$ mice depends at least in part on intrinsic defects or on non-cell-autonomous effects, meaning lack of support from $Ank^{KI/KI}$ osteoblasts for osteoclastogenesis, we performed mCOB–BMM cocultures. We analyzed mineral resorption on osteologic slides and found that cocultures of $Ank^{+/+}$ mCOBs with $Ank^{+/+}$ BMMs had the most mineralized area resorbed, while cocultures of $Ank^{KI/KI}$ mCOBs with $Ank^{KI/KI}$ BMMs had the least (Fig. 6E), as was expected. Replacement of $Ank^{KI/KI}$ with $Ank^{+/+}$ mCOBs or BMMs partially restored the percentage of resorbed area. The fact that

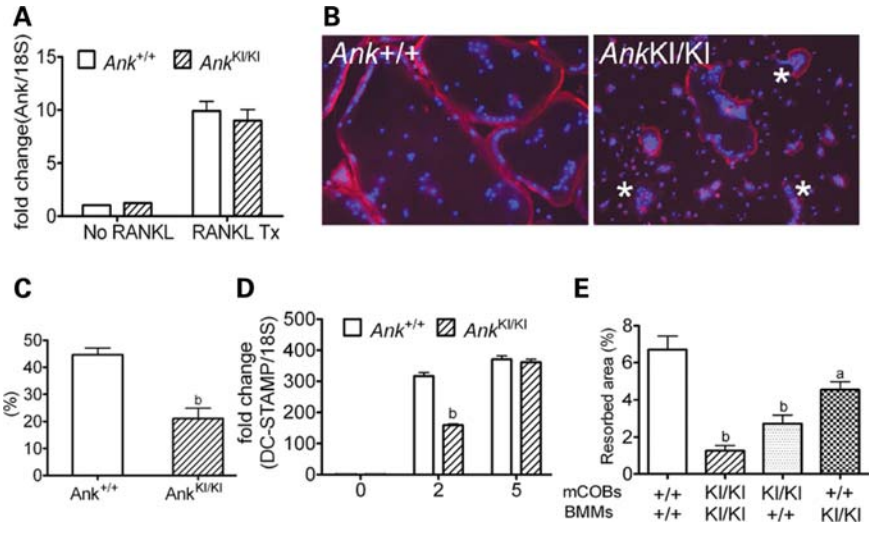

Figure 6. *In vitro* murine osteoclast assays. (**A**) Increased *Ank* mRNA in mature $Ank^{+/+}$ and $Ank^{KI/KI}$ BMM cultures by qPCR. (**B**) Rhodamine-phalloidin staining of actin and DAPI nuclear staining of mature osteoclasts. Note the disrupted actin belt (*) in $Ank^{KI/KI}$ BMMs, which are generally smaller in area. (**C**) Decreased fusion efficiency (percentage of nuclei number in mature osteoclasts to total number of nuclei in culture) of $Ank^{KI/KI}$ BMMs. $^{b}P < 0.01$. (**D**) qPCR of *DC-Stamp* expression in BMMs during osteoclastogenesis. Decreased *DC-Stamp* mRNA level in day 2 $Ank^{KI/KI}$ BMM cultures containing pre-fusion osteoclasts. $^{b}P < 0.01$. (**E**) Cocultures of primary mCOBs and BMMs. Resorption assay evaluated after 12 days of plating on calcium-phosphate coated slides. Replacement with $Ank^{+/+}$ mCOBs or $Ank^{+/+}$ BMMs partially rescues resorption activity of $Ank^{KI/KI}$ mCOB or $Ank^{KI/KI}$ BMM cultures, respectively (one-way ANOVA with Tukey's multiple-comparison to the $Ank^{+/+}$ mCOB-$Ank^{+/+}$ BMM group, $^{a}P < 0.05$; $^{b}P < 0.01$). There is no significant difference between replacement with $Ank^{KI/KI}$ mCOB or $Ank^{KI/KI}$ BMM cultures.

resorption capability of $Ank^{KI/KI}$ osteoclasts is only partially rescued suggests that reduced osteoclastogenesis of $Ank^{KI/KI}$ cultures is caused by a combination of cell-autonomous effects and reduced osteoblast-mediated osteoclastogenesis.

Mcsf and *Rankl*, which stimulate osteoclastogenesis, and *Opg*, which suppresses osteoclast differentiation, are the best-described signals transferred from osteoblasts to osteoclasts (43,44). We first examined *Mcsf*, *Rankl* and *Opg* expression in RNAs isolated from osteoblasts as well as in RNAs isolated from calvarial and femoral bones. We detected no significant differences in cells and bones between $Ank^{+/+}$ and $Ank^{KI/KI}$ mice (Supplementary Material, Fig. S3A and Table S2). Next, we measured the concentration of RANKL in conditioned media from mCOBs–BMM cocultures by the ELISA assay and found no significant difference in all different combinations of cocultures (Supplementary Material, Fig. S3B). Moreover, the resorption rate of the $Ank^{KI/KI}$ mCOB–$Ank^{KI/KI}$ BMM cocultures grown on calcium-phosphate slides was not rescued by supplementing with 10 ng/ml and 30 ng/ml RANKL (Supplementary Material, Fig. S3C). Taken together, we suspect that the impaired interaction between $Ank^{KI/KI}$ osteoblasts and osteoclasts is not due to lack of *Rankl* expression.

Bone marrow transplantation partially rescues the bone mass phenotype of $Ank^{KI/KI}$ mice

The most direct means to study the contribution of osteoclasts to the CMD phenotype *in vivo* are bone marrow transplant (BMT) rescue experiments. We transplanted 4-week-old male donor bone marrow from $Ank^{+/+}$ and $Ank^{KI/KI}$ mice into same age $Ank^{+/+}$ and $Ank^{KI/KI}$ recipient mice. Donor mice expressed GFP driven by an MHC Class I, H-$2k^{b}$ promoter to obtain GFP-selectable bone marrow cells. Eight weeks after BMT, we confirmed that all mice reached 80–90% chimerism in peripheral blood by FACS analysis for H-$2k^{b}$-GFP positive donor cells (data not shown). In $Ank^{KI/KI}$ mice, which had received $Ank^{+/+}$ bone marrow, we found a partial rescue of the high bone mass phenotype in mandibles, in cortical width of calvariae and a reduction of diaphyseal trabeculation in femurs by μCT analysis (Fig. 7, Supplementary Material, Table S3). Another phenotype of $Ank^{KI/KI}$ mice, the flared shape of metaphyses and decreased tissue density in femoral cortical bones were not corrected (Supplementary Material, Table S3). However, rescue of bone shape could not be expected as bone shape is already fully developed in 4-week-old mice. Tissue density remained unchanged, which indicates that bone mineral quality is not controlled by the osteoclast phenotype. Furthermore, $Ank^{+/+}$ mice receiving $Ank^{KI/KI}$ bone marrow showed a tendency of increased bone mass in calvarial, mandibular and femoral bones, although some parameters did not reach significant differences compared with $Ank^{+/+}$ mice that had received $Ank^{+/+}$ bone marrow. This may be due to high biological variability between animals or an insufficient recovery period. In conclusion, this data suggests that abnormal osteoclasts partially contribute to the increased bone mass phenotype in $Ank^{KI/KI}$ mice.

DISCUSSION

This study was intended to better describe the pathogenic mechanism leading to a CMD-like phenotype in the Phe377del *Ank* KI mouse model, which replicates features

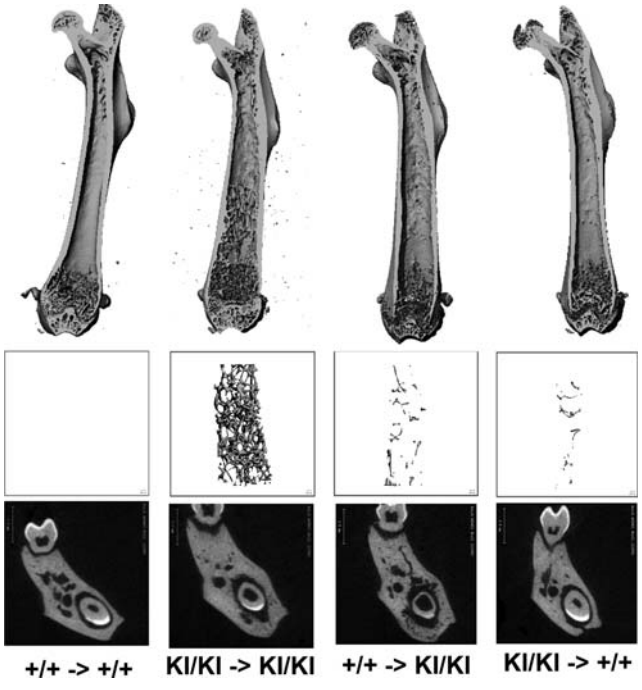

Figure 7. μCT analysis of femurs and mandibles after BMT. Images show longitudinal sections of femurs highlighting the bone shape, trabeculation in diaphyseal region and cross-section through mandibles. $Ank^{+/+}$ (+/+) and $Ank^{KI/KI}$ (KI/KI) bone marrow transplanted (→) into $Ank^{+/+}$ and $Ank^{KI/KI}$ recipient mice ($Ank^{+/+} \rightarrow Ank^{+/+}$ mice, $n = 8$; $Ank^{KI/KI} \rightarrow Ank^{KI/KI}$ mice, $n = 6$; $Ank^{+/+} \rightarrow Ank^{KI/KI}$ mice, $n = 8$; $Ank^{KI/KI} \rightarrow Ank^{+/+}$ mice, $n = 6$). $Ank^{+/+}$ BMT partially rescued the high mandibular bone mass of $Ank^{KI/KI}$ mandibles. The trabeculation in diaphyses of $Ank^{KI/KI}$ femurs was reduced in the group of $Ank^{KI/KI}$ mice receiving $Ank^{+/+}$ bone marrow and slightly increased in $Ank^{+/+}$ mice that received $Ank^{KI/KI}$ bone marrow.

of CMD patients on a morphological, cellular and serological level. Because of its rarity, CMD has been understudied and while we could confirm some of the mouse data by *in vitro* studies with cells from CMD patients, other data will need to be confirmed in follow-up experiments with tissues or cells from CMD patients as they become available.

To study the effect of CMD mutant ANK on osteoblast differentiation and mineralization, we used mCOB and mouse BMSCs representing osteoblasts from craniofacial bones and from long bones. We had previously shown a significantly higher serum level of total ALP in $Ank^{KI/KI}$ mice (28); however, the ALP staining was comparable between $Ank^{+/+}$ and $Ank^{KI/KI}$ calvarial osteoblast cultures. ALP is found primarily in liver and bone but is also produced by intestine, kidney and placenta. Paradoxically, we observed decreased ALP staining in $Ank^{KI/KI}$ BMSC cultures. Although increased serum ALP is often used as a biochemical marker for high bone turnover, it is not a bone-specific marker due to high cross-reactivity with liver ALP. ALP staining from osteoblast cultures appears to be more indicative for bone mineralization than serum ALP in these mice. However, the cellular heterogeneity in cultures should also be considered. We believe that decreased ALP-stained colonies in $Ank^{KI/KI}$ BMSC cultures correlate with decreased numbers of attached colonies as shown by crystal violet staining, which raises the possibility of a shift in mesenchymal cell populations of bone marrow in $Ank^{KI/KI}$ mice.

We determined the mineralization potential of mouse osteoblasts with von Kossa staining, which shows the binding of phosphate to silver and alizarin red, which specifically chelates with calcium. Both assays showed less mineralized nodules in $Ank^{KI/KI}$ mCOB and BMSC cultures than in $Ank^{+/+}$ cultures suggesting that the *Ank* Phe377deletion mutation suppresses osteoblast mineralization. These *in vitro* data reflect the hypomineralized skeletal phenotype of $Ank^{KI/KI}$ mice. Since bone samples from CMD patients rarely become available, detailed examination of bone quality and mineralization has never been reported. Literature references to sclerotic cranial bone are based on high radiopacity of radiographic images, which may be based on craniofacial hyperostosis rather than on hypermineralization of normal thickness bone. In fact, Elcioglu and Hall (15) report hypomineralization in one of their patients.

We hypothesized that the Phe377del mutation in ANK causes abnormal mineralization (i) by disrupting the physiological concentration of ePPi or (ii) by altering expression of genes that regulate mineralization in osteoblasts. A recent biochemical study used a sensitive radioflux method to test the transport activity of mutant ANK proteins in frog oocytes and showed greatly reduced PPi transport in ANK carrying CMD mutations (C331R and C389R) (27). Surprisingly, we detected no difference in the ePPi levels between $Ank^{+/+}$ and $Ank^{KI/KI}$ calvarial osteoblasts but found that the enzymatic activity of PC-1 in $Ank^{KI/KI}$ calvarial osteoblasts was significantly increased. Higher PC-1 activity is expected to generate more ePPi. At normal concentrations, ePPi acts as a regulator of HA crystal formation and at high concentrations promotes CPPD formation as seen in chondrocalcinosis patients. Previously, we showed by wide-angle X-ray diffraction that no CPPD crystals are present in $Ank^{KI/KI}$ tibiae or scapulae, indirectly suggesting that ePPi levels in $Ank^{KI/KI}$ bone were not excessively high (28). Based on these data, we propose that mutant ANK is likely to transport less PPi into the extracellular matrix and that the ePPi level in $Ank^{KI/KI}$ osteoblasts is maintained by increased PC-1 activity.

In the late stage of osteoblast differentiation but not in early stages of osteoblastogenesis of $Ank^{KI/KI}$ mCOB cultures, the expression of genes including *Mmp13*, *Ocn*, *Runx2* and *Osx* was reduced. In addition, we found decreased *Phex* expression in $Ank^{KI/KI}$ calvarial osteoblasts. Inactivating mutations of *Phex* result in hypophosphatemia and hypomineralization in XLH patients and in *Hyp* mice (29–32). These data are in line with our earlier findings that mineralization is decreased in $Ank^{KI/KI}$ osteoblast cultures and in bone of $Ank^{KI/KI}$ mice and suggest that the Phe377del Ank mutation affects gene expression during osteoblastogenesis.

A recent study showed that the conditional deletion of *Phex* in osteoblasts alone is sufficient to reproduce hypophosphatemia and to increase serum FGF23 in *Hyp* mice (45). Since *Phex* was decreased in $Ank^{KI/KI}$ calvarial osteoblast cultures, we examined the expression of *Fgf23* and found that the level in calvarial osteoblast cultures was very low without significant differences between $Ank^{+/+}$ and $Ank^{KI/KI}$ cultures. In *Hyp* mice, PHEX is absent in osteoblasts but FGF23 levels increase only when osteoblasts differentiate into osteocytes (34,38). Therefore, we decided to examine *Fgf23* levels directly in calvarial and femoral bones, which contain

osteocytes and observed significant increases of *Fgf23* expression in calvariae as well as in femurs of $Ank^{KI/KI}$ mice.

FGF23 is known as a phosphaturic $1,25(OH)_2D_3$-regulating hormone that controls phosphorus homeostasis and bone mineralization. FGF23 binds to FGF receptors (mainly FGFR1) and the coreceptor KLOTHO in the kidney promotes excretion of Pi and reduces 1α-hydroxylase activity, which leads to reduced serum Pi and $1,25\text{-}(OH)_2D_3$ levels. We found lower serum calcium and phosphate levels in 6-week-old $Ank^{KI/KI}$ male mice with the difference between the $Ank^{+/+}$ and the $Ank^{KI/KI}$ groups being statistically significant. Literature reports of serum calcium and phosphorus levels in CMD patients are inconsistent (5,10,17,18,46). Increased *Fgf23* can regulate the $Ank^{KI/KI}$ bone phenotype through bone-kidney axis or local effects on bone cells. There is increasing evidence that FGF23 can directly affect skeletal mineralization, independent of phosphorus homeostasis (35). In a preliminary study, we did not find kidney malfunctions or gross-histological differences in kidney morphology in 10-week-old $Ank^{KI/KI}$ male mice. To our knowledge, FGF23 serum levels have not been studied in CMD patients. More detailed studies examining the roles of increased *Fgf23* on bone homeostasis in $Ank^{KI/KI}$ mice through local or systemic effects are needed.

Osteoclasts are multinucleated resorptive cells derived from the monocyte-macrophage lineage (47). In $Ank^{KI/KI}$ BMM cultures, we detected significantly reduced numbers of multinucleated osteoclasts and a stark reduction in mineral resorption. When we compared osteoclast cultures derived from peripheral blood of CMD patients to age- and gender-matched healthy control subjects, we also found decreased numbers of multinucleated osteoclasts and reduced mineral resorption in cultures derived from CMD patients. At a first glance, these *in vitro* experiments seem to be conflicting to our *in vivo* data, which showed increased serum TRAP levels and increased osteoclast numbers in $Ank^{KI/KI}$ mice (28). However, we believe that the increased osteoclast numbers compensate for dysfunctional osteoclasts, which are unable to resorb bone at a normal rate. The reduced resorption capability of osteoclasts in $Ank^{KI/KI}$ mice and CMD patients may explain the hyperostotic phenotype of craniofacial bones and extensive trabeculation in diaphyses.

Several processes are required for mature osteoclasts to resorb bone, including attachment of osteoclasts to bone matrix, formation of the sealing zone and ruffled border, polarization of the plasma membrane, synthesizing and trafficking acids and enzymes onto resorbed bone surface. Our studies showed that reduced osteoclastogenesis in $Ank^{KI/KI}$ BMM cultures may depend on at least three features: (i) reduced fusion and migration capability; (ii) disrupted actin ring formation; and (iii) abnormal osteoblast–osteoclast communication.

The dendritic cell-specific seven-transmembrane protein (DC-STAMP) is an essential factor for cell–cell fusion in osteoclasts. Studies using DC-STAMP-deficient mice have shown that multinucleation is a prerequisite for osteoclast activity (48,49). These DC-STAMP-deficient mice only produce mononuclear osteoclasts and suffer from osteopetrosis due to reduced bone resorption. We plated equal numbers of $Ank^{+/+}$ and $Ank^{KI/KI}$ BMMs in parallel cultures and found that fewer nuclei fused to form mature osteoclasts in $Ank^{KI/KI}$ cultures, meaning the ratio of mononuclear cells to multinucleated cells (more than three nuclei) was higher in $Ank^{KI/KI}$ cultures. We consistently detected delayed expression of *DC-Stamp* in $Ank^{KI/KI}$ pre-fusion osteoclasts. Moreover, our live-cell imaging data provided evidence of decreased mobility of $Ank^{KI/KI}$ cells, which may contribute to reduced frequency of fusion. Subsequently, we doubled or quadrupled the cell density and observed increased formation of multinucleated osteoclasts (data not shown). Multinucleated syncytia that developed in $Ank^{KI/KI}$ BMM cultures, however, did not spread out and migrate which may negatively affect their resorption activity. Taken together, our *in vitro* experiments suggest a complex osteoclast phenotype in $Ank^{KI/KI}$ BMMs and provide convincing evidence for linking mutant ANK to migration defects.

Osteoclasts attach to bone matrix during resorption and undergo cellular reorganization resulting in the formation of an actin ring structure known as sealing zone, which surrounds the ruffled border. The sealing zone interacts tightly with the bone surface via integrin heterodimeric receptors and provides an acidic environment between resorption lacunae and extracellular fluid secreted from osteoclasts. Disruption of the sealing zone leads to defective bone resorption and to an osteopetrotic phenotype in $Pyk2^{-/-}$ mice (50). Destaing *et al.* (51) demonstrated that podosome organization and actin polymerization are a highly dynamic process by using live confocal imaging and fluorescence recovery after photobleaching analysis in single osteoclasts expressing actin GFP. In addition, regulation of sealing zone formation is a complex process and involves podosome-associated proteins, adapter proteins, kinases, Rho GTPase and enzymes (52,53). We observed disrupted actin staining of $Ank^{KI/KI}$ BMMs but whether the ANK mutation affects actin turnover directly or cell signals associated with actin remodeling remains to be determined. Nonetheless, these data support our hypothesis that the ANK Phe377del mutation causes a cell-autonomous defect in $Ank^{KI/KI}$ osteoclasts.

BMT studies have shown some successful engraftment of normal bone marrow in osteopetrosis patients resulting in amelioration of symptoms after transplantation (54,55). We expected that replacing abnormal osteoclasts with wild-type cells in $Ank^{KI/KI}$ mice can partially correct the skeletal phenotype. Since the pathogenesis of $Ank^{KI/KI}$ mice involves not just bone resorption by osteoclasts, full rescue is unlikely to be achieved by BMT, especially if the recipient mice are older. Eight weeks after transplantation into 4-week-old recipient mice, we started to detect decreased bone mass in hyperostotic mandibles and correction of extensive trabeculation in diaphyses in $Ank^{KI/KI}$ mice that had received $Ank^{+/+}$ bone marrow. The age when mice receive the transplant is important to achieve the optimal rescue effects. Adult mice and rats with congenital osteosclerosis (oc/oc mice) have not shown significant improvements after BMT (56,57), whereas neonatal mice, even with only 20% replacement efficiency, showed some degree of rescue (58). A case report showed that a successful hematopoietic engraftment performed in a child at the age of 8 years failed to correct osteopetrosis, which may be due to the late attempt of transplantation (59). Most osteopetrosis patients are transplanted under the age of 2 years (54,55).

In summary, we have identified defects in both osteoblasts and osteoclasts in $Ank^{KI/KI}$ mice, a mouse model for CMD. To date, treatment for CMD patients is very limited and surgery appears to be the only option for patients with life-threatening symptoms. Our studies have uncovered that in addition to impaired function in mesenchymal cells, the CMD-causing ANK mutation also affects osteoclasts, which can be a target for treatment. Further studies are needed to determine whether BMT performed at young age may be able to delay cranial hyperostosis and therefore neurological symptoms for CMD patients with a severe skeletal phenotype.

MATERIALS AND METHODS

Mice

$Ank^{KI/KI}$ mice carrying a human CMD mutation [a deletion of $TTC_{1130-1132}$ (phenylalanine 377) in exon 9 of *Ank*] were generated in the Gene Targeting and Transgenic Facility (GTTF) at the University of Connecticut Health Center (UCHC). Mice were bred from a 129/Sv into a C57Bl/J6 background (N5). Detailed *in vivo* skeletal characterization of this CMD mouse model was previously published (28). $Ank^{null/null}$ mice (26) were maintained in a mixed background of FVB and C57Bl/J6 (kindly provided by Dr David Kingsley, Stanford University). All work involving animals was approved by the Animal Care Committee (ACC) of UCHC.

Mouse calvarial osteoblast cultures (mCOBs)

Calvariae from postnatal day 4–7 mice were isolated and digested with 0.05% trypsin (Invitrogen–Gibco) and 0.15% collagenase (Type II; Sigma Aldrich) for four cycles (20 min/cycle) at 37°C. Only cells from digests 2–4 were collected. Cells were plated at a density of 10 000 per cm^2 in DMEM (Invitrogen–Gibco) and cultured until confluent. Cells were then maintained in osteoblast differentiating medium (α-MEM; Invitrogen–Gibco) containing 10% fetal bovine serum (FBS; Hyclone), 100 IU/ml penicillin, 100 μg/ml streptomycin (Invitrogen–Gibco), 50 μg/ml ascorbic acid and 4 mM β-glycerophosphate (Sigma). The medium was changed every 2–3 days.

Mouse bone marrow stromal cell cultures (mBMSCs)

mBMSCs were prepared as previously described (60). Briefly, epiphyseal growth plates of femurs were cut off and bone marrow was flushed out from the shafts of femurs, tibia and humeri of 7–9-week-old mice. Cell suspension was filtered through a 70 μm cell strainer and cells were cultured in α-MEM with 10% FBS at a density of 3×10^6 cells/well in 6-well culture plates. At day 3, half of the medium was replaced with fresh α-MEM. On day 7, cells were switched to α-MEM containing 10% FBS, 100 IU/ml penicillin, 100 μg/ml streptomycin, 50 μg/ml ascorbic acid and 8 mM β-glycerophosphate to induce osteoblast differentiation. Medium was changed every other day.

Matrix expression and mineralization assays in osteoblast cultures

We determined matrix expression and mineral deposition in osteoblast cultures by ALP staining and von Kossa/alizarin red S staining, respectively. ALP staining was performed using a commercially available ALP kit (Sigma) according to the manufacturer's instructions. To visualize mineral nodule formation, osteoblast cultures were stained with 5% silver nitrate solution while exposed to light for 30 min before washing with distilled water. To validate results from von Kossa staining, cells were stained with alizarin red S (AR-S, 40 mM, pH 4.2) for 10 min. AR-S-stained nodules were then extracted by adding 10% (w/v) cetylpyridinium chloride in 10 mM sodium phosphate and incubated for 30 min at room temperature on a shaking platform. The concentration of the AR-S extract was then determined by absorbance measurement at 562 nm as described (61).

Extracellular pyrophosphate assay

ePPi levels of cultured osteoblasts were measured by a modified radiometric method (21,62,63). This PPi assay uses a UDPG pyrophosphorylase reaction in a system with phosphoglucomutase, glucose-6-phosphate dehydrogenase (G6PDH) and 6-phosphogluconate dehydrogenase to form NADPH. The PPi level was determined by differential adsorption on activated charcoal of UDP-D-[6-^{3}H] glucose from its PPi-catalyzed reaction product 6-phospho [6-^{3}H] gluconate. Sodium pyrophosphate (Fisher Scientific) was used to establish a standard curve (0–10 μM). PPi was equalized for the DNA content determined by the PicoGreen assay (Molecular Probes) and statistical analysis was performed using Student's *t*-test. Osteoblasts from $Ank^{null/null}$ mice were used as control for lack of pyrophosphate transport by ANK.

Enzymatic activity of TNAP and PC-1

For the measurement of TNAP activity, cell lysate was added to a substrate solution containing 15 mM 4-nitrophenyl phosphate in 1 M diethanolamine and 0.5 mM $MgCl_2$, pH 9.8 (Sigma). The reaction product (p-nitrophenol) was determined colorimetrically by absorbance measurement at 405 nm. To determine the PC-1 activity, cell lysate was added to HEPES-buffered DMEM (25 mM HEPES, pH 7.4) containing 1 mM p-znitrophenyl-thymidine monophosphate (Sigma) and incubated at 37°C for 1 h. The reaction was stopped by adding 0.1 M NaOH, and optical density was read at 405 nm. The TNAP and PC-1 activity was normalized to the total protein concentration of the cell lysate as determined by BCA protein assay (Pierce).

RNA analysis

Total RNA from cultured cells or bone tissues was isolated with TRIzol (Invitrogen) according to the manufacturer's instructions. RNA was treated with DNase I (Invitrogen) and cDNA was synthesized using Superscript II reverse transcriptase (Invitrogen). qPCR using iTaq SYBR Green Supermix with ROX (BioRad) was performed in an ABI-7300

Table 1. Amplification primers for quantitative real-time PCR

Gene	Forward primer	Reverse primer
Tnap	5′-GCTGATCATTCCCACGTTTT-3′	5′-CTGGGCCTGGTAGTTGTTGT-3′
Ank	5′-CTGCTGCTACAGAGGCAGTG-3′	5′-GACAAAACAGAGCGTCAGCGA-3′
Bsp	5′-CAGAGGAGGCAAGCGTCACT-3′	5′-CTGTCTGGGTGCCAACACTG-3′
ColI	5′-ACGTCCTGGTGAAGTTGGTC-3′	5′-CAGGGAAGCCTCTTTCTCCT-3′
Enpp1	5′-CGCCACCGAGACTAAA-3′	5′-AGGAATCATAGCGTCCG-3′
Mmp13	5′-GCAGTTCCAAAGGCTACAA-3′	5′-ATAGGGCTGGGTCACACTT-3′
Ocn	5′-AAGCAGGAGGGCAATAAGGT-3′	5′-TTTGTAGGCGGTCTTCAAGC-3′
Sp7(Osx)	5′-GGATGGCGTCCTCTCTGCTTGAG-3′	5′-GAGGAGTCCATTGGTGCTTGAGA-3′
Phex	5′-GCATGATTAACCAGTATAGCAA-3′	5′-GGTCTATAGGAATTGCACCTTAC-3′
Runx2	5′-ACCTAGTTTGTTCTCTGATCGCCT-3′	5′-GGGATCTGTAATCTGACTCTGTCCTT-3′
Fgf23	5′-ACTTGTCGCAGAAGCATC-3′	5′-GTGGGCGAACAGTGTAGAA-3′
Mepe	5′-ACTATCCACAAGTGGCCTCG-3′	5′-CCGCTGTGACATCCCTTTAT-3′
Dmp1	5′-GCGCGGATAAGGATGA-3′	5′-GTCCCCGTGGCTACTC-3′
DC-Stamp	5′-CTAGCTGGCTGGACTTCATCC-3′	5′-TCATGCTGTCTAGGAGACCTC-3′
Rankl	5′-CACCATCAGCTGAAGATAGT-3′	5′-CCAAGATCTCTAACATGACG-3′
Mcsf	5′-ATTCTATGCTGGGCACACAGGACT-3′	5′-ATCCTCCAGCCCTTTCTCTTTGGT-3′
Opg	5′-AGAGCAAACCTTCCAGCTGC-3′	5′-CTGCTCTGTGGTGAGGTTCG-3′
18S	5′-TTGACGGAAGGGCACCACCAG-3′	5′-GCACCACCACCCACGGAATCG-3′

instrument (Applied Biosystems). PCR efficiency was optimized and primer specificity was tested by melting curve analysis. Relative quantification of gene expression was determined by the ΔΔCt method and 18S RNA was used for data normalization. PCR primer sequences are listed in Table 1.

Phosphate, calcium and PTH measurement

Blood for serum analysis in mice was collected from the submandibular vein using animal lancets (Goldenrod; Medipoint) from 6- and 10-week-old male animals after 12 h food and water deprivation. Total serum calcium and phosphate was determined using a calcium reagent kit (Eagle Diagnostics) and a Phosphorus Liquid UV kit (Stanbio), respectively. Serum PTH levels were measured using a two-sided enzyme-linked immunosorbent assay (ELISA) specific for intact mouse PTH (Immutopics).

Intramuscular bone explantation

Intramuscular bone explantation was performed as described (37,38). Femurs from 4.5-day-old newborn mice were isolated under a dissecting microscope and explanted into the paralateral back muscles of 4-week-old male $Ank^{+/+}$ and $Ank^{KI/KI}$ recipient mice ($n = 6$ per group). Bones were radiographically documented prior to explantation. Animals were anesthetized by injecting ketamine/xylazine (150/10 mg/kg body weight) intraperitoneally. One femur of a donor mouse was explanted into an $Ank^{+/+}$ mouse and the other femur into an $Ank^{KI/KI}$ mouse. Each host mouse received one $Ank^{+/+}$ femur in the left back muscle and one $Ank^{KI/KI}$ femur in the contralateral back muscle. Buprenex (0.08 mg/kg) was given for post-operative pain control. Three weeks after surgery, explanted bones were harvested, radiographed and examined by computed microtomography (μCT) in the MicroCT facility at UCHC (mCT20; ScanCo Medical AG, Bassersdorf, Switzerland). Diaphyseal trabeculation was measured 1.8 mm below the growth plate over a 2 mm distance.

Murine osteoclast cultures

We used three different mouse osteoclast cultures. Murine macrophage-like RAW264.7 cells were grown in α-MEM (10% FBS, 100 IU/ml penicillin, 100 μg/ml streptomycin) with RANKL (30 ng/ml; R&D Systems) to stimulate osteoclast differentiation. Enriched osteoclast progenitors were prepared by FACS with surface markers to obtain a $CD11b^{-/low}CD45R^{-}CD3^{-}CD115^{high}$ subpopulation in bone marrow from $Ank^{+/+}$ and $Ank^{KI/KI}$ mice (39). We used commercially available antibodies directly conjugated to various fluorochromes (eBioscience) and sorting was performed in a FACS Aria instrument (Becton Dickinson). Mouse BMM cultures were obtained from bone marrow flushed out from femora and tibia of 7–9-week-old mice and cultured for 18–24 h in α-MEM containing 10% FBS (Hyclone), 100 IU/ml penicillin and 100 μg/ml streptomycin (Invitrogen–Gibco). Non-adherent cells were collected and purified by Ficoll separation (Lymphoprep, Axis Shield, Oslo, Norway). Sorted cell populations and BMM cultures were treated with M-CSF only (30 ng/ml; R&D Systems) or M-CSF and RANKL (30 ng/ml) for 5 days to stimulate osteoclast differentiation. For all cultures, cells were seeded at a density of 5000 cells/well on 96-well culture plates for osteoclast assays or 2×10^5 cells/well on 6-well plates for RNA isolation.

Osteoclasts derived from human peripheral blood

All work involving human subjects was approved by the UCHC Institutional Review Board. Blood was obtained from healthy controls and CMD patients. Peripheral blood mononuclear cells were isolated as described (64). Briefly, 8 ml of whole blood was diluted with an equal amount of PBS, layered over 10 ml Ficoll with a density of 1.077 (Lymphoprep) and centrifuged at 800*g* for 30 min (without break) to precipitate red blood cells. The interface, containing mononuclear cells was collected, diluted with a 3-fold volume of PBS and centrifuged at 290*g* for 10 min.

Pellets were resuspended in 0.83% NH_4Cl to lyze red blood cells whenever contamination from red blood cells was observed. After counting, cells were plated at a density of 3×10^5 cells/well on 96-well plates in α-MEM supplemented with 30 ng/ml human M-CSF, 30 ng/ml RANKL, 5 ng/ml TGF-β1 (R&D Systems) and 1 μM dexamethasone for 15–17 days for TRAP staining and 19 days for resorption assays.

In vitro osteoclast assays

Osteoclast formation and resorption were analyzed by TRAP staining and resorption assays using osteologic discs as described previously (28). F-actin rings of mature osteoclasts were examined by rhodamine–phalloidin staining (Invitrogen–Molecular Probes). Mature BMMs (day 5 in culture) were washed twice with PBS and fixed with 2.5% glutaraldehyde. Cells were then washed with PBS and permeabilized with ethanol/acetone (1:1) for 30 s at room temperature. After washing with PBS, cells were stained with rhodamine–phalloidin (1:40 dilution in PBS) for 25 min in the dark. Hoechst 33342 dye (trihydrochloride trihydrate; Molecular Probes; 1:1000 in PBS) was used for nuclear staining. Images were taken by a Z1 Observer microscope (Zeiss, Germany). Experiments were performed in triplicate and repeated at least three times.

Live-cell imaging

We performed live-cell imaging on BMM cultures. Briefly, $Ank^{+/+}$ and $Ank^{KI/KI}$ BMMs were cultured with MCSF and RANKL (30 ng/ml) for 2 days before placing the dish on a temperature- and CO_2-controlled stage (37°C; 6% CO_2) using a Z1 Observer Microscope and an Axiocam MRc camera (Zeiss, Germany). Three-minute time-lapse images of $Ank^{+/+}$ and $Ank^{KI/KI}$ BMM cultures were taken over a period of 6 h alternating between $Ank^{+/+}$ and $Ank^{KI/KI}$ BMM cultures over 4 days. AxioVision Rel 4.7 software was used to create AVI movies from image stacks. Quantitative measurement of migratory velocity was performed using MetaMorph software (Molecular Devices).

Cocultures of mCOBs and BMMs

mCOBs were prepared from 4- to 7-day-old mice and BMMs were obtained from 7- to 9-week-old mice as described. Osteoblasts (5000 cells/well on osteologic slides; BD Biosciences) were plated 1 day prior to adding BMMs (5000 cells/well). Cocultures were maintained in osteogenic medium (α-MEM with 10% FBS, 50 μg/ml ascorbic acid and 4 mM β-glycerophosphate) supplemented with 10^{-11} M $1\alpha,25(OH)_2D_3$ and 10^{-7} M dexamethasone. Cultures on osteologic slides were stained with von Kossa after 12 days in culture to determine resorptive activity.

Bone marrow transplantation

We used 4-week-old male donor and recipient mice to generate bone marrow chimera. $Ank^{+/+}$ and $Ank^{KI/KI}$ donor mice (N10 for C57Bl6) were obtained by crossing $Ank^{+/KI}$ mice with transgenic mice overexpressing GFP driven by a MHC Class I, H-$2k^b$ promoter to obtain GFP-selectable bone marrow cells. To cause myeloablation, recipient mice were irradiated by giving 11 Gy administered in two split doses of 5.5 Gy each in an interval of 4–5 h. To rescue hematopoiesis, recipient mice were injected with 10×10^6 bone marrow cells from donor femurs through retro-orbital injection in a 100 μl volume 4–5 h after the second irradiation. Eight weeks after transplantation, the degree of chimerism was confirmed by FACS analysis for GFP. Skulls, mandibles and femurs were evaluated by X-ray radiography and computed microtomography (μCT) in the MicroCT facility at UCHC (mCT20; ScanCo Medical AG). Calvariae were analyzed over an area of 100 slices using the sagittal suture of the central parietal region as reference point. Mandibular data were collected by measuring vertical sections at the mandibular foramen. Metaphyseal trabecular measurements of femurs were taken at the distal growth plate in 80 consecutive slices of 12 μm resolution over a distance of 960 μm. Diaphyseal trabeculation in femurs was determined 2.4 mm from growth plate (200 slices) and extending 3.6 mm (300 slices). Volumetric regions were rendered as three-dimensional arrays with an isometric voxel dimension of 12 μm. Fifty cross-sectional slices of 12 μm in the mid-diaphysis were used to calculate cortical bone parameters.

Statistical analysis

Statistical analysis was performed using Prism 5 software (GraphPad Software).

SUPPLEMENTARY MATERIAL

Supplementary Material is available at *HMG* online.

ACKNOWLEDGEMENTS

We are indebted to members of the UCHC Bone Group and Dr William Mohler at UCHC for their helpful discussions. We wish to thank the UCHC μCT facility for their support.

Conflict of Interest statement. None declared.

FUNDING

The project was supported by institutional funding and grant AR49539 (NIH) to E.J.R. and M01RR006192 (GCRC).

REFERENCES

1. Jackson, W.P.U., Albright, F., Drewery, G., Hanelin, J. and Rubin, M.L. (1954) Metaphyseal dysplasia, epiphyseal dysplasia, diaphyseal dysplasia and related conditions. *Arch. Intern. Med.*, **94**, 871–885.
2. Hayashibara, T., Komura, T., Sobue, S. and Ooshima, T. (2000) Tooth eruption in a patient with craniometaphyseal dysplasia: case report. *J. Oral. Pathol. Med.*, **29**, 460–462.
3. Mintz, S. and Velez, I. (2004) Craniometaphyseal dysplasia associated with obstructive sleep apnoea syndrome. *Dentomaxillofac. Radiol.*, **33**, 262–266.

4. Zhang, H., Somerman, M.J., Berg, J., Cunningham, M.L. and Williams, B. (2007) Dental anomalies in a child with craniometaphysial dysplasia. *Pediatric Dentistry*, **29**, 415–419.
5. Cheung, V.G., Boechat, M.I. and Barrett, C.T. (1997) Bilateral choanal narrowing as a presentation of craniometaphyseal dysplasia. *J. Perinatol.*, **17**, 241–243.
6. Ramseyer, L.T., Leonard, J.C. and Stacy, T.M. (1993) Bone scan findings in craniometaphyseal dysplasia. *Clin. Nucl. Med.*, **18**, 137–139.
7. Haverkamp, F., Emons, D., Straehler-Pohl, H.J. and Zerres, K. (1996) Craniometaphyseal dysplasia as a rare cause of a severe neonatal nasal obstruction. *Int. J. Pediatr. Otorhinolaryngol.*, **34**, 159–164.
8. Franz, D.C., Horn, K.L. and Aase, J. (1996) Craniometaphyseal dysplasia: operative findings and treatment. *Am. J. Otol.*, **17**, 283–287.
9. Beighton, P., Hamersma, H. and Horan, F. (1979) Craniometaphyseal dysplasia—variability of expression within a large family. *Clin. Genet.*, **15**, 252–258.
10. Richards, A., Brain, C., Dillon, M.J. and Bailey, C.M. (1996) Craniometaphyseal and craniodiaphyseal dysplasia, head and neck manifestations and management. *J. Laryngol. Otol.*, **110**, 328–338.
11. Day, R.A., Park, T.S., Ojemann, J.G. and Kaufman, B.A. (1997) Foramen magnum decompression for cervicomedullary encroachment in craniometaphyseal dysplasia: case report. *Neurosurgery*, **41**, 960–964.
12. Cai, C., Zhang, Q., Shen, C., Sun, G. and Wang, C. (2008) Chiari malformation caused by craniometaphyseal dysplasia: case report and review of literature. *Eur. J. Pediatr. Surg.*, **18**, 198–201.
13. Halliday, J. (1949) A rare case of bone dystrophy. *Br. J. Surg.*, **37**, 52–63.
14. Millard, D.R. Jr, Maisels, D.O., Batstone, J.H. and Yates, B.W. (1967) Craniofacial surgery in craniometaphyseal dysplasia. *Am. J. Surg.*, **113**, 615–621.
15. Elcioglu, N. and Hall, C.M. (1998) Temporal aspects in craniometaphyseal dysplasia: autosomal recessive type. *Am. J. Med. Genet.*, **76**, 245–251.
16. Key, L.L. Jr, Volberg, F., Baron, R. and Anast, C.S. (1988) Treatment of craniometaphyseal dysplasia with calcitriol. *J. Pediatr.*, **112**, 583–587.
17. Fanconi, S., Fischer, J.A., Wieland, P., Giedion, A., Boltshauser, E., Olah, A.J., Landolt, A.M. and Prader, A. (1988) Craniometaphyseal dysplasia with increased bone turnover and secondary hyperparathyroidism: therapeutic effect of calcitonin. *J. Pediatr.*, **112**, 587–591.
18. Yamamoto, T., Kurihara, N., Yamaoka, K., Ozono, K., Okada, M., Yamamoto, K., Matsumoto, S., Michigami, T., Ono, J. and Okada, S. (1993) Bone marrow-derived osteoclast-like cells from a patient with craniometaphyseal dysplasia lack expression of osteoclast-reactive vacuolar proton pump. *J. Clin. Invest.*, **91**, 362–367.
19. Reichenberger, E., Tiziani, V., Watanabe, S., Park, L., Ueki, Y., Santanna, C., Baur, S.T., Shiang, R., Grange, D.K., Beighton, P. *et al.* (2001) Autosomal dominant craniometaphyseal dysplasia is caused by mutations in the transmembrane protein ANK. *Am. J. Hum. Genet.*, **68**, 1321–1326.
20. Nurnberg, P., Thiele, H., Chandler, D., Hohne, W., Cunningham, M.L., Ritter, H., Leschik, G., Uhlmann, K., Mischung, C., Harrop, K. *et al.* (2001) Heterozygous mutations in ANKH, the human ortholog of the mouse progressive ankylosis gene, result in craniometaphyseal dysplasia. *Nat. Genet.*, **28**, 37–41.
21. Ho, A.M., Johnson, M.D. and Kingsley, D.M. (2000) Role of the mouse ank gene in control of tissue calcification and arthritis. *Science*, **289**, 265–270.
22. Okawa, A., Nakamura, I., Goto, S., Moriya, H., Nakamura, Y. and Ikegawa, S. (1998) Mutation in Npps in a mouse model of ossification of the posterior longitudinal ligament of the spine. *Nat. Genet.*, **19**, 271–273.
23. Fedde, K.N., Blair, L., Silverstein, J., Coburn, S.P., Ryan, L.M., Weinstein, R.S., Waymire, K., Narisawa, S., Millan, J.L., MacGregor, G.R. *et al.* (1999) Alkaline phosphatase knock-out mice recapitulate the metabolic and skeletal defects of infantile hypophosphatasia. *J. Bone Miner. Res.*, **14**, 2015–2026.
24. Sweet, H.O. and Green, M.C. (1981) Progressive ankylosis, a new skeletal mutation in the mouse. *J. Hered.*, **72**, 87–93.
25. Hakim, F.T., Cranley, R., Brown, K.S., Eanes, E.D., Harne, L. and Oppenheim, J.J. (1984) Hereditary joint disorder in progressive ankylosis (ank/ank) mice. I. Association of calcium hydroxyapatite deposition with inflammatory arthropathy. *Arthritis Rheum.*, **27**, 1411–1420.
26. Gurley, K.A., Chen, H., Guenther, C., Nguyen, E.T., Rountree, R.B., Schoor, M. and Kingsley, D.M. (2006) Mineral formation in joints caused by complete or joint-specific loss of ANK function. *J. Bone Miner. Res.*, **21**, 1238–1247.
27. Gurley, K.A., Reimer, R.J. and Kingsley, D.M. (2006) Biochemical and genetic analysis of ANK in arthritis and bone disease. *Am. J. Hum. Genet.*, **79**, 1017–1029.
28. Chen, I.P., Wang, C.J., Strecker, S., Koczon-Jaremko, B., Boskey, A. and Reichenberger, E.J. (2009) Introduction of a Phe377del mutation in ANK creates a mouse model for craniometaphyseal dysplasia. *J. Bone Miner. Res.*, **24**, 1206–1215.
29. Francis, F. (1995) A gene (PEX) with homologies to endopeptidases is mutated in patients with X-linked hypophosphatemic rickets. The HYP Consortium. *Nat. Genet.*, **11**, 130–136.
30. Du, L., Desbarats, M., Viel, J., Glorieux, F.H., Cawthorn, C. and Ecarot, B. (1996) cDNA cloning of the murine Pex gene implicated in X-linked hypophosphatemia and evidence for expression in bone. *Genomics*, **36**, 22–28.
31. Liu, S., Brown, T.A., Zhou, J., Xiao, Z.S., Awad, H., Guilak, F. and Quarles, L.D. (2005) Role of matrix extracellular phosphoglycoprotein in the pathogenesis of X-linked hypophosphatemia. *J. Am. Soc. Nephrol.*, **16**, 1645–1653.
32. Onishi, T., Okawa, R., Ogawa, T., Shintani, S. and Ooshima, T. (2007) Phex mutation causes the reduction of npt2b mRNA in teeth. *J. Dent. Res.*, **86**, 158–162.
33. Larsson, T., Marsell, R., Schipani, E., Ohlsson, C., Ljunggren, O., Tenenhouse, H.S., Juppner, H. and Jonsson, K.B. (2004) Transgenic mice expressing fibroblast growth factor 23 under the control of the alpha1(I) collagen promoter exhibit growth retardation, osteomalacia, and disturbed phosphate homeostasis. *Endocrinology*, **145**, 3087–3094.
34. Liu, S., Tang, W., Zhou, J., Stubbs, J.R., Luo, Q., Pi, M. and Quarles, L.D. (2006) Fibroblast growth factor 23 is a counter-regulatory phosphaturic hormone for vitamin D. *J. Am. Soc. Nephrol.*, **17**, 1305–1315.
35. Sitara, D., Kim, S., Razzaque, M.S., Bergwitz, C., Taguchi, T., Schuler, C., Erben, R.G. and Lanske, B. (2008) Genetic evidence of serum phosphate-independent functions of FGF-23 on bone. *PLoS Genet.*, **4**, e1000154.
36. Wang, H., Yoshiko, Y., Yamamoto, R., Minamizaki, T., Kozai, K., Tanne, K., Aubin, J.E. and Maeda, N. (2008) Overexpression of fibroblast growth factor 23 suppresses osteoblast differentiation and matrix mineralization *in vitro*. *J. Bone Miner. Res.*, **23**, 939–948.
37. Tanaka, H. and Seino, Y. (2004) Direct action of 1,25-dihydroxyvitamin D on bone: VDRKO bone shows excessive bone formation in normal mineral condition. *J. Steroid Biochem. Mol. Biol.*, **89–90**, 343–345.
38. Liu, S., Tang, W., Zhou, J., Vierthaler, L. and Quarles, L.D. (2007) Distinct roles for intrinsic osteocyte abnormalities and systemic factors in regulation of FGF23 and bone mineralization in Hyp mice. *Am. J. Physiol. Endocrinol. Metab.*, **293**, E1636–E1644.
39. Jacquin, C., Gran, D.E., Lee, S.K., Lorenzo, J.A. and Aguila, H.L. (2006) Identification of multiple osteoclast precursor populations in murine bone marrow. *J. Bone Miner. Res.*, **21**, 67–77.
40. Jurdic, P., Saltel, F., Chabadel, A. and Destaing, O. (2006) Podosome and sealing zone: specificity of the osteoclast model. *Eur. J. Cell Biol.*, **85**, 195–202.
41. Takahashi, N., Akatsu, T., Udagawa, N., Sasaki, T., Yamaguchi, A., Moseley, J.M., Martin, T.J. and Suda, T. (1988) Osteoblastic cells are involved in osteoclast formation. *Endocrinology*, **123**, 2600–2602.
42. Suda, T., Takahashi, N. and Martin, T.J. (1992) Modulation of osteoclast differentiation. *Endocr. Rev.*, **13**, 66–80.
43. Henriksen, K., Neutzsky-Wulff, A.V., Bonewald, L.F. and Karsdal, M.A. (2009) Local communication on and within bone controls bone remodeling. *Bone*, **44**, 1026–1033.
44. Matsuo, K. and Irie, N. (2008) Osteoclast-osteoblast communication. *Arch. Biochem. Biophys.*, **473**, 201–209.
45. Yuan, B., Takaiwa, M., Clemens, T.L., Feng, J.Q., Kumar, R., Rowe, P.S., Xie, Y. and Drezner, M.K. (2008) Aberrant Phex function in osteoblasts and osteocytes alone underlies murine X-linked hypophosphatemia. *J. Clin. Invest.*, **118**, 722–734.
46. Sheppard, W.M., Shprintzen, R.J., Tatum, S.A. and Woods, C.I. (2003) Craniometaphyseal dysplasia: a case report and review of medical and surgical management. *Int. J. Pediatr. Otorhinolaryngol.*, **67**, 71–77.
47. Udagawa, N., Takahashi, N., Akatsu, T., Tanaka, H., Sasaki, T., Nishihara, T., Koga, T., Martin, T.J. and Suda, T. (1990) Origin of osteoclasts: mature monocytes and macrophages are capable of differentiating into osteoclasts under a suitable microenvironment prepared by bone marrow-derived stromal cells. *Proc. Natl Acad. Sci. USA*, **87**, 7260–7264.

48. Yagi, M., Miyamoto, T., Sawatani, Y., Iwamoto, K., Hosogane, N., Fujita, N., Morita, K., Ninomiya, K., Suzuki, T., Miyamoto, K. *et al.* (2005) DC-STAMP is essential for cell–cell fusion in osteoclasts and foreign body giant cells. *J. Exp. Med.*, **202**, 345–351.
49. Yagi, M., Miyamoto, T., Toyama, Y. and Suda, T. (2006) Role of DC-STAMP in cellular fusion of osteoclasts and macrophage giant cells. *J. Bone Miner. Metab.*, **24**, 355–358.
50. Gil-Henn, H., Destaing, O., Sims, N.A., Aoki, K., Alles, N., Neff, L., Sanjay, A., Bruzzaniti, A., De Camilli, P., Baron, R. *et al.* (2007) Defective microtubule-dependent podosome organization in osteoclasts leads to increased bone density in Pyk2(−/−) mice. *J. Cell. Biol.*, **178**, 1053–1064.
51. Destaing, O., Saltel, F., Geminard, J.C., Jurdic, P. and Bard, F. (2003) Podosomes display actin turnover and dynamic self-organization in osteoclasts expressing actin-green fluorescent protein. *Mol. Biol. Cell*, **14**, 407–416.
52. Bruzzaniti, A. and Baron, R. (2006) Molecular regulation of osteoclast activity. *Rev. Endocr. Metab. Disord.*, **7**, 123–139.
53. Luxenburg, C., Parsons, J.T., Addadi, L. and Geiger, B. (2006) Involvement of the Src-cortactin pathway in podosome formation and turnover during polarization of cultured osteoclasts. *J. Cell Sci.*, **119**, 4878–4888.
54. Driessen, G.J., Gerritsen, E.J., Fischer, A., Fasth, A., Hop, W.C., Veys, P., Porta, F., Cant, A., Steward, C.G., Vossen, J.M. *et al.* (2003) Long-term outcome of haematopoietic stem cell transplantation in autosomal recessive osteopetrosis: an EBMT report. *Bone Marrow Transplant.*, **32**, 657–663.
55. Gerritsen, E.J., Vossen, J.M., Fasth, A., Friedrich, W., Morgan, G., Padmos, A., Vellodi, A., Porras, O., O'Meara, A., Porta, F. *et al.* (1994) Bone marrow transplantation for autosomal recessive osteopetrosis. A report from the Working Party on Inborn Errors of the European Bone Marrow Transplantation Group. *J. Pediatr.*, **125**, 896–902.
56. Popoff, S.N. and Marks, S.C. Jr (1991) Congenitally osteosclerotic (os/os) rabbits are not cured by bone marrow transplantation from normal littermates. *Am. J. Anat.*, **192**, 274–280.
57. Seifert, M.F. and Marks, S.C. Jr (1987) Congenitally osteosclerotic (oc/oc) mice are resistant to cure by transplantation of bone marrow or spleen cells from normal littermates. *Tissue Cell*, **19**, 29–37.
58. Johansson, M., Jansson, L., Ehinger, M., Fasth, A., Karlsson, S. and Richter, J. (2006) Neonatal hematopoietic stem cell transplantation cures oc/oc mice from osteopetrosis. *Exp. Hematol.*, **34**, 242–249.
59. Nicholls, B.M., Bredius, R.G., Hamdy, N.A., Gerritsen, E.J., Lankester, A.C., Hogendoorn, P.C., Nesbitt, S.A., Horton, M.A. and Flanagan, A.M. (2005) Limited rescue of osteoclast-poor osteopetrosis after successful engraftment by cord blood from an unrelated donor. *J. Bone Miner. Res.*, **20**, 2264–2270.
60. Kalajzic, I., Kalajzic, Z., Kaliterna, M., Gronowicz, G., Clark, S.H., Lichtler, A.C. and Rowe, D. (2002) Use of type I collagen green fluorescent protein transgenes to identify subpopulations of cells at different stages of the osteoblast lineage. *J. Bone Miner. Res.*, **17**, 15–25.
61. Stanford, C.M., Jacobson, P.A., Eanes, E.D., Lembke, L.A. and Midura, R.J. (1995) Rapidly forming apatitic mineral in an osteoblastic cell line (UMR 106–01 BSP). *J. Biol. Chem.*, **270**, 9420–9428.
62. Lust, G. and Seegmiller, J.E. (1976) A rapid, enzymatic assay for measurement of inorganic pyrophosphate in biological samples. *Clin. Chim. Acta Int. J. Clin. Chem.*, **66**, 241–249.
63. Zaka, R., Stokes, D., Dion, A.S., Kusnierz, A., Han, F. and Williams, C.J. (2006) P5L mutation in Ank results in an increase in extracellular inorganic pyrophosphate during proliferation and nonmineralizing hypertrophy in stably transduced ATDC5 cells. *Arthritis Res. Ther.*, **8**, R164.
64. Susa, M., Luong-Nguyen, N.H., Cappellen, D., Zamurovic, N. and Gamse, R. (2004) Human primary osteoclasts: *in vitro* generation and applications as pharmacological and clinical assay. *J. Transl. Med.*, **2**, 6.